Characterizations of combustion destabilization in an axisymmetric supersonic cavity-based combustor

Qinyuan Li, Bo Yan, Mingbo Sun, Jiajian Zhu, Yifu Tian*, Minggang Wan, Tiangang Luo, Yongchao Sun*

Abstract

Three-dimensional characterizations and evolution laws of the flame structure during combustion destabilization in an axisymmetric supersonic combustor were investigated. The multi-view OH-PLIF imaging system was used to visualize the instantaneous flame structures distributing at multiple typical cross-sections of a fully transparent axisymmetric supersonic glass combustor. The high-speed photography and pressure measurement systems were employed to assist in the analysis of the flame structure evolution during combustion destabilization. The experiments were conducted with an inflow speed of Mach 2.5 and a total temperature of 1800 K. The global equivalence ratios (GER) were 0.12, 0.15, 0.21 and 0.26, respectively. It was found that a loop-shaped flame with a central hole is an essential flame structure characterization in the axisymmetric supersonic combustor. The flame loop mainly distributes near the cavity shear-layer, and the instantaneous structure fluctuates over time. There is the most intense combustion and thickened flame near the cavity ramp. As GER exceeds 0.21, an excessive enhanced combustion induces thermal choking. The flame propagates upstream away from the cavity along the boundary-layer near the jet wake. It leads to a violent reciprocal flame propagation, marking an unsteady combustion. The thermal choking initiates near the ramp where the most intense combustion occurs. The local flame loop is significantly expanded, filling almost the entire flow path. The loop-shaped flame structure downstream the combustor is affected slightly due to a low-speed and thickened cavity shear-layer. In contrast, the flame structure near the middle part of the combustor is disrupted severely. A diffused and fragmented flame loop fluctuates violently over time. A large amount of fragmented flames spread into the core flow occasionally.

Keywords: *scramjet, axisymmetric supersonic combustor, combustion destabilization, flame structure, OH-PLIF*

1. Introduction

Scramjet is a key technology for hypersonic cruise flight and cheap near-Earth orbit transport [1-4]. Supersonic combustor is a vital element that release heat and improve thrust performance[5,6]. Achieving a steady and efficient combustion is one of the technical challenges due to a supersonic and strongly turbulent environment in the combustor[7-10]. Reducing flow rates is an essential solution, which includes utilizing the combustor configurations with cavity[11-13] or struct[14-16]. The cavity-based combustor does not intrude into the supersonic main flow that efficiently reduces total pressure loss[17,18]. The low-speed and high-temperature recirculation flow in the cavity improves the combustion conditions significantly[19-22]. The fuel/air mixing is promoted by the cavity shear-layer generated by the interactions with the low-speed recirculation flow and high-speed main flow[23-25]. Therefore, the cavity is widely used in scramjet.

The cavity-based supersonic combustor with rectangular cross-section is disturbed by the corner boundary-layer effect that tends to trigger combustion destabilization. The strong flow separation near the corner enhances the local heat release that is easily to induce thermal choking[26-28]. Axisymmetric combustor configuration is an important design scheme to solve this dilemma. The circular cross-section without sharp corner efficiently eliminates the corner boundary layer. Furthermore, this type of combustor is advanced by the low structural weight, low wetted surface and strong structural strength[29-31]. The utilizing of axisymmetric supersonic cavity-based combustors is valued nowadays.

Despite such advances, the combustion destabilization induced by thermal choking is still a difficulty that plagues the robust operation for combustor. Liu et al.[32] found that the thermal choking

initiates downstream the cavity where the combustion hear release is comparable with the relief of flow channel area. The flame propagates upstream with the forming of thermal throat, which leads to a scram-to-ram mode transition. Despite some relatively steady combustion modes with specific conditions can be achieved through thermal choking, the unsteady mode transition with combustion oscillation is a common phenomenon over a wide range of operating conditions[22,33,34]. Investigation of the combustion destabilization induced by thermal choking is increasingly emphasized. Scholars[32,35-37] have studied some typical combustion modes in axisymmetric supersonic combustor through OH-PLIF visualization. A loop-shaped flame with a hole near the center is discovered indirectly. It can be deduced that the flame loop is expanded and the central hole tends to be closed as thermal choking occurs. Baccarella et al.[38] have studied the dynamics of the interactions between isolator and combustor during thermal choking. They found that the pseudo-normal shock upstream propagation in combustor is affected by the flow oscillation in isolator, but no feedback from the combustor was observed.

Flame structure visualization is an essential way to clarify the characterizations of combustion destabilization in an axisymmetric supersonic cavity-based combustor. The three-dimensional characterizations of flame distribution in an axisymmetric combustor have not been fully captured because of a lack of multi-view imaging. Although quite a few excellent teams have studied the issue directly or indirectly, the evolution of flame structure from steady to unsteady combustion have not been revealed directly due to the limitation of visualization conditions.

In order to reveal the three-dimensional characterizations and evolution laws of the flame structure during combustion destabilization, a multi-view OH-PLIF imaging system was used to visualize the instantaneous flame structure distributing on multiple typical planes in a fully transparent axisymmetric supersonic glass combustor. The axial and circumferential flame planar structures in the combustor were analyzed. Furthermore, the high-speed photography and pressure measurement systems were utilized to clarify the combustion stability to assist in the analysis of the flame structure evolution during the combustion destabilization.

2. Experimental system

As shown in Fig. 1, the experimental system consists of a direct-connected supersonic combustion experimental system, a fully transparent axisymmetric supersonic glass combustor, a multi-view OH-PLIF imaging system, a high-speed photography system and a pressure measurement system. The direct-connected supersonic combustion system generated a high-enthalpy supersonic airflow using a Laval nozzle and the combustion of alcohol, oxygen, and air. The Mach number, total temperature, and mass flow rate of the supersonic flow were 2.5, 1800 K, and 400 g/s, respectively. The axisymmetric supersonic combustor included a cavity and a diffuser section, which was made by a fully transparent quartz glass combustor and enabled multi-view optical visualization of the flame. The diameter of the supersonic channel upstream of the cavity was 35 mm. The depth and length of the cavity were 11 mm and 62 mm, respectively. The distance between the leading edge and the front of the ramp was 35.4 mm. The inclination angle of the ramp was 22.5°. The hydrogen fuel was injected into the supersonic flow at an inclination angle of 90° through 8 circumferentially distributed injectors. It had a diameter of 1.0 mm and was 128 mm upstream of the leading edge. The diffusion section with a length of 294 mm and a dilatation angle of 2° was connected downstream of the cavity. The global equivalence ratio (GER) during the experiments were 0.12, 0.15, 0.21 and 0.26. Each experiment was repeated 3 times with specific GER.

A multi-view OH-PLIF imaging system was utilized to visualize the instantaneous flame structures distributing at multiple typical cross-sections of the axisymmetric supersonic combustor. A pumping laser beam with the wavelength of 283.5 nm was generated by a 10 Hz pump laser system (Nd: YAG), which was directed into a dye laser (PrecisionScan, Sirah Lasertechnik) to produce a laser beam with the wavelength of 566 nm. Then, a frequency doubling unit was used to generate a laser beam with 283.55 nm wavelength and 4 mJ/pulse energy, which is able to excite the ground-state OH radicals to emit fluorescent signals. To visualize the instantaneous flame planar structure, the laser beam is modulated into a laser sheet with 100 mm width and 500 μm thickness by 1 concave lens (f = -15 mm) and 2 convex lenses (f = +290 mm and f = +500 mm). The OH-PLIF signals were captured by an ICMOS imaging camera (TRICAM Lambert GEV_B2020M) to generate with a gate width of 70 ns. A 310±11 nm filter was utilized to improve the image signal-to-noise ratio. A timing controller (DG645)

was employed to ensure that the camera shutter is opened precisely when the OH-PLIF signals are generated.

The instantaneous flame planar structures at 3 typical cross-sections were visualized through adjusting the position of laser sheet, as shown in Fig. 1. The axial flame structure was captured when the laser sheet passed through the symmetry axis of the combustor. The circumferential flame structures distributing at the cross-section I and II were visualized when the laser sheet was adjusted to be vertical to the symmetry axis of the combustor. The two cross-sections were located at the middle part of the combustor and near the ramp, separately. The cross-section I was 20 mm from the cavity leading edge. The cross-section II was 3.4 mm from the front of ramp. Since the ICMOS camera lens could not aim squarely to the laser sheet, its optical axis had to be aimed at an angle to the imaged region. A mirror was used to reflect the OH-PLIF signals to the ICMOS camera in a limited experimental space. The skewed viewing angles caused a distortion of the OH-PLIF images. A nonlinear interpolation algorithm was used to correct the image distortion.

A high-speed photography system was used to capture the chemiluminescence image sequence over a broadband spectrum. The image sequence represented the dynamic characterizations of the flame propagation and oscillations over time. The frame rate and exposure time of the high-speed camera (FASTCAM SA-X2) were 20 kHz and 50 μs, respectively.

A pressure measurement system (Pressure System Inc.9116) was used to measure the axial wall static pressure. There were 16 measurement points distributing along the axial direction, as illustrated by the red points in Fig. 1. The measurement frequency and accuracy were 500 Hz and ±0.05%, respectively.

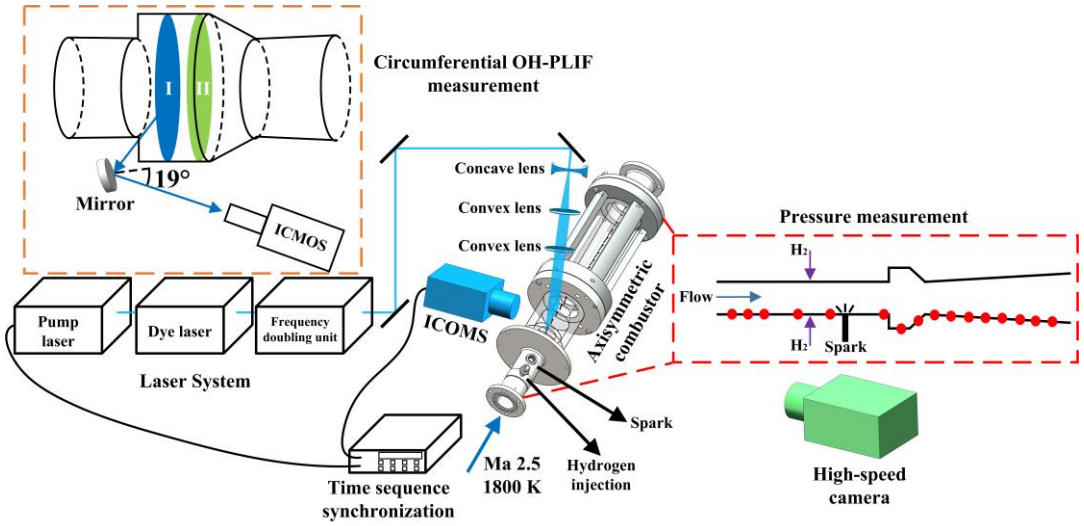

Fig. 1 Schematic diagram of the experimental system.

3. Research results

Fig. 2 displays the wall pressure distribution varies with increasing GER. The pressure at each measurement point is the time-averaged wall static pressure. It illustrates that the peak of pressure is always near the ramp whether in non-reaction flow or combustion flows. When the combustion occurs as GER = 0.12, the pressure inside and upstream the cavity is dramatically increased. It indicates that the combustion establishes a strong backpressure in these regions. The combustion is enhanced with increasing GER, which is reflected by the increased pressure and expanded high-pressure region. The pressure increase is limited as GER is elevated to 0.15. The combustion still occurs in the region where the cavity is located. However, the high-pressure region is expanded upstream when GER = 0.21, which means that the flame propagates upstream away from the cavity. As indicated by Liu et al.[32], the excessive addition of heat release cannot match the expansion of combustor area, which leads to thermal choking that promotes the flame propagation upstream. The pressure peak at the ramp suggests that thermal choking initiates near the ramp. The pressure is further increased accompanied by the expanded high-pressure region when GER is increased to 0.26. The thermal choking is further exacerbated.

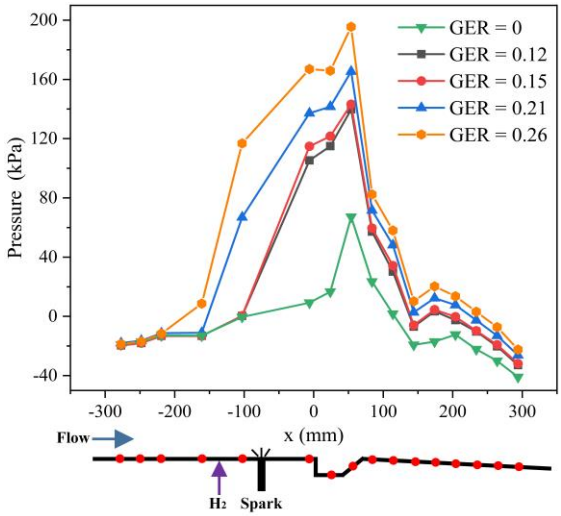

Fig. 2 Wall pressure distribution along axial direction with various GER.

The intensity of flame chemiluminescence radiation with various GER versus time curves are illustrated in Fig. 3. It is able to reflect the stability of combustion. The fluctuation of intensity curve is relatively slight when GER is less than 0.15, which suggests that the combustion is approximately steady. Fig. 2 illustrates that the combustion occurs mainly in the region where the cavity is located. It is largely supported by the flame holding effects of the cavity[29,30]. The intensity is decreased as GER reaches 0.21 as a result of the combustion occurring upstream the cavity. The intensity curve presents a tendency to oscillating. Since the flame propagates upstream away from the cavity induced by thermal choking as illustrated in Fig. 2, the contribution of the cavity to the combustion stabilization is diminished. It leads to a combustion destabilization accompanied by the intensity oscillation over time. In actual, the curve with GER = 0.21 represents a violently reciprocal flame propagation. The increasing to peak values indicates that the flame propagates downstream to the cavity region. In contrast, the decreasing to valley values indicates a flame propagates upstream away from the cavity. The oscillation is enhanced significantly when GER is further increased to 0.26. Thus, the excessive enhanced combustion induces a combustion destabilization with a violently reciprocal flame propagation.

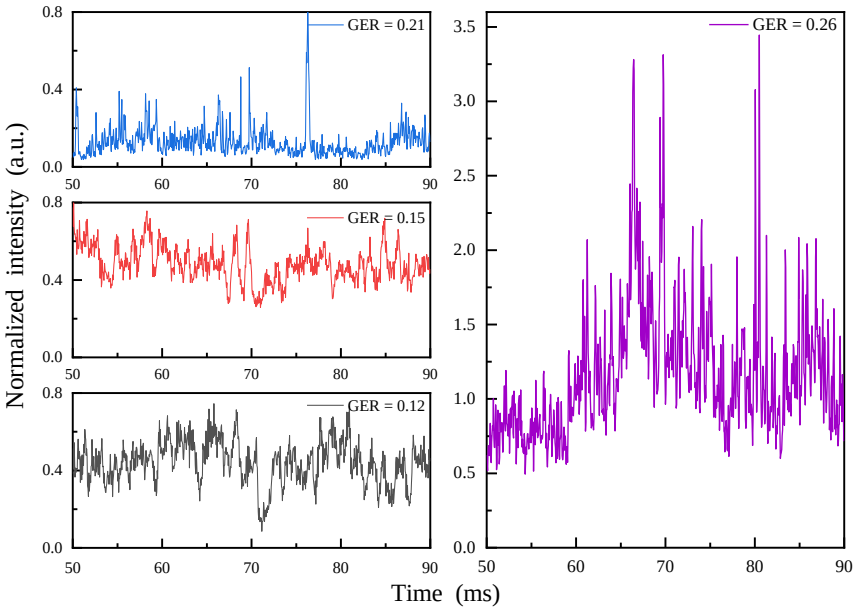

Fig. 3 Intensity-time curves of flame chemiluminescence radiation with various GER.

The instantaneous and time-averaged axial OH-PLIF images are presented in Fig. 4. It illustrates the characterization of flame planar structure distributing along the axial direction. The flame mainly distributes near the cavity shear-layer and is thickened along the axial direction. It impinges the ramp

and spreads into the cavity recirculation flow downstream. The core flow exists in the space between the flames on either side. It is a high-speed flow that is unfavorable for flame stabilization. The initial burning portion named flame base is near the cavity leading edge during the combustion with GER = 0.12. There is a violent interaction between the fuel jets and thermal products from the cavity recirculation flow. The flame base keeps an approximately steady combustion there and continues to release heat products downstream the cavity shear-layer[19,20]. Thus, a cavity shear-layer flame is formed, and the structure fluctuates relatively slightly compared to higher GER. As GER is increased to 0.15, the instantaneous flame structure shows that the flame propagates forth and back constantly. When the cavity shear-layer flame is thickened significantly, which suggests that the local combustion conditions are improved, the flame is promoted to propagate upstream along the hydrogen jet wake near the boundary-layer. It can be seen that the flame thickness near the jet wake upstream the cavity is restricted compared to the downstream cavity shear-layer flame due to the lack of assisting from the recirculation flow. It is hard for the local flame base to maintain a steady combustion. The cavity shear-layer flame is thinning simultaneously that the local combustion environment becomes deteriorated. Therefore, the flame base propagates downstream. In summary, the flame propagates reciprocally with a higher GER. Nevertheless, the combustion with GER = 0.15 is still be considered as an approximately steady combustion. Fig. 2 indicates that the flame is not far from the cavity, resulting a limited intensity fluctuation as shown in Fig. 3. When GER exceeds 0.21, the flame distributing along the jet wake is more thickened than GER =0.15. Fig. 2 suggests that the flame propagates upstream to a considerable distance from the cavity. However, the flame further forward than 25.5 mm upstream the cavity cannot be visualized due to the limited length of the transparent region. Since the flame base appears away from the cavity, where the thickness of boundary-layer is more thinning and the impact of high-speed flow is much more powerful, the combustion destabilization occurs indicated by Fig. 3. The thickened and thinned flame near the jet wake reflects a reciprocal flame propagation. The heat products marked by OH near the cavity shear-layer and inside the cavity indicates that the cavity still plays an important role in maintaining the combustion.

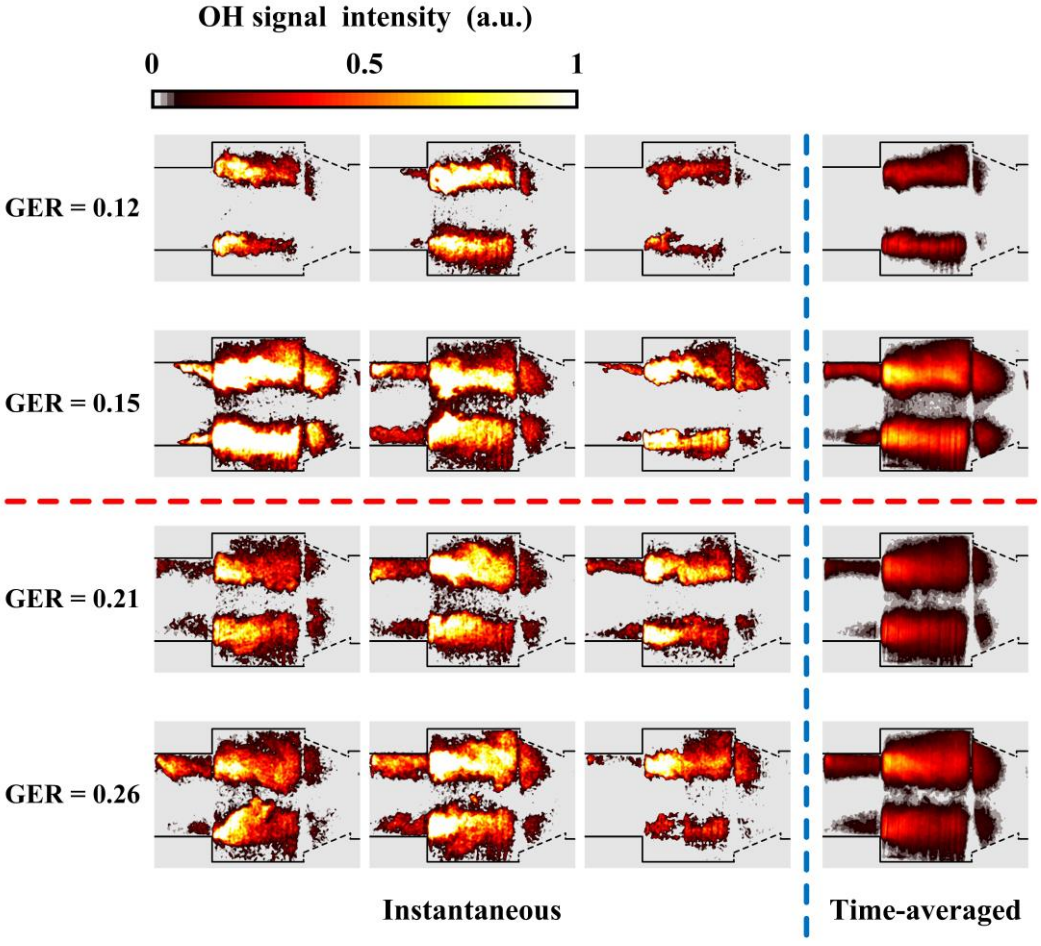

Fig. 4 Instantaneous and time-averaged axial OH-PLIF images.

Vanyai et al.[37] found that the flame distributes in a loop-shaped region at the exit of the axisymmetric supersonic combustor. It can be deduced that there is also a loop-shaped flame inside the combustor. As shown in Fig. 5, the instantaneous circumferential flame structure appears as an irregular loop inside the combustor at the middle and rear section, which matches the visualization results discovered by Vanyai et al. The green dashed loop in the figure represents the projection of the cavity leading edge, which can be regarded as a reference line near the cavity shear-layer. The loop-shaped cavity recirculation region is between the green dashed loop and the circular boundaries of the image. As our previous study[39], the axisymmetric supersonic combustor generates a loop-shaped cavity shear-layer that is beneficial for combustion and forms a flame loop. The periphery of the flame loop exhibits a twisted and wrinkled morphology due to the disturbance of the turbulence. The first to be discussed is the flame structure at the middle section of the combustor. The thickness of the cavity shear-layer is limited there, forming a relatively narrow flame loop distributing roughly near the projection of the cavity leading edge. The hollow region inside the flame loop is the core flow. Only some fragmented flames distribute in this region due to the difficulty of stabilizing combustion in the high-speed core flow. The fragmented flames also exist outside the flame loop, which means that the midstream part of cavity recirculation is detrimental to stabilize the combustion, even though the local flow rate is slow. The analysis above indicates that the combustion is relatively stable when GER is less than 0.15. The OH distribution at the middle section is relatively continuous, and the flame loop is structurally integrated. The increased GER enhances the combustion, expanding the flame loop toward the cavity and core flow. However, when GER exceeds 0.21, the thermal choking induces combustion destabilization. The flame propagates upstream and away from the cavity, leading to an obvious decrease in the OH-PLIF signal intensity. Although the irregular flame loop is still maintained, the structure is more fragmented, and the morphology is changed more drastically over time.

The cavity shear-layer is thicker downstream, which enables a more intense combustion and expands the flame distribution. Compared to the middle section of the combustor, the combustion is enhanced, and the flame loop at the rear section is widely spread. The cavity is almost filled with flame. The core flow marked by the central hollow region is compressed sharply. Besides, a large amount of fragmented flames appear there. It means that the speed in the core flow is decreased markedly. When GER is increased more than 0.21, despite a fragmented flame loop at the middle section due to the reciprocal flame propagation, the structure of flame loop still keeps integrity at the rear section. In summary, a more favorable environment for combustion is generated near the ramp, as evidenced by the enhanced combustion, wider spreading flame loop, and more integrated flame structure.

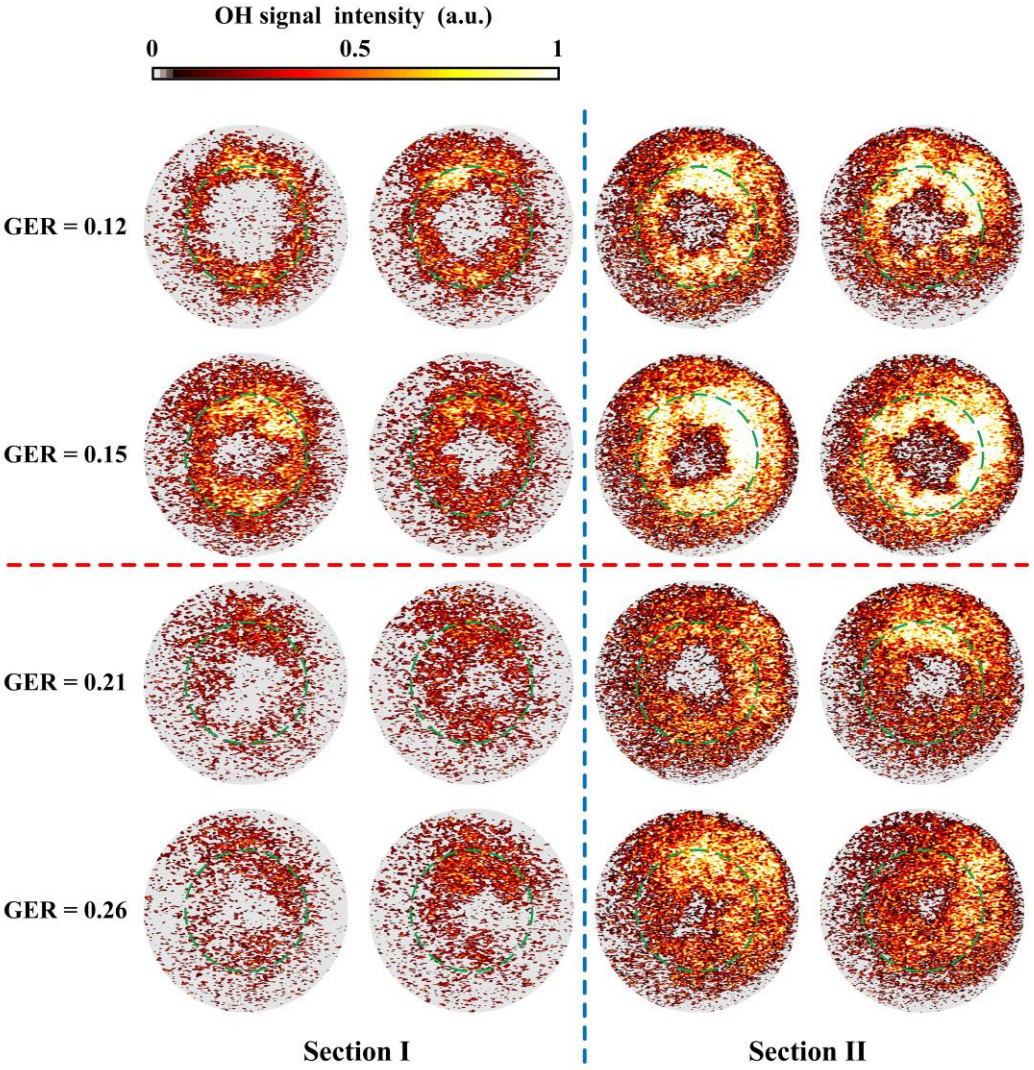

Fig. 5 Instantaneous circumferential OH-PLIF images at the middle and rear cross-sections.

Fig. 6 is the distribution of instantaneous OH-PLIF signal intensity centers. It is similar to the concept of mass center in mechanics. The solution methods for the intensity center in any instantaneous OH-PLIF image in the polar coordinate system are as follows:

$$I(r) = \int rI(r,\theta)d\theta \tag{1}$$

$$r_c/R = \frac{1}{R}\frac{\int rI(r)dr}{\int I(r)dr} \tag{2}$$

$$I(\theta) = \int rI(r,\theta)dr \tag{3}$$

$$\theta_c = \frac{\int \theta I(\theta)d\theta}{\int I(\theta)d\theta} \tag{4}$$

where (r_c, θ_c) are the polar coordinates of the intensity centers; I is the local intensity of OH-PLIF; R is the distance between the symmetry axis and the bottom of cavity.

Although the combustion intensity and flame distribution are affected deeply by GER and the position of the combustor, all of the intensity centers distribute mainly in the narrow loop-shaped region that is centered on the projection of cavity leading edge (r/R = 0.6) and its half-width is only nearly 5%. It indicates that the distribution of the intensity centers is a relatively stable property of the

combustion in an axisymmetric supersonic combustor. The distribution of intensity centers with GER = 0.15 is more concentrated than GER = 0.12. However, they are diffused again as thermal choking occurs induced by increasing GER. It suggests that the combustion stability is enhanced with an appropriate elevation of GER before thermal choking occurring. A more aggregated distribution of the intensity centers at the rear section is presented, compared to the middle section. It suggests that the flame instantaneous structure near the ramp is more steady.

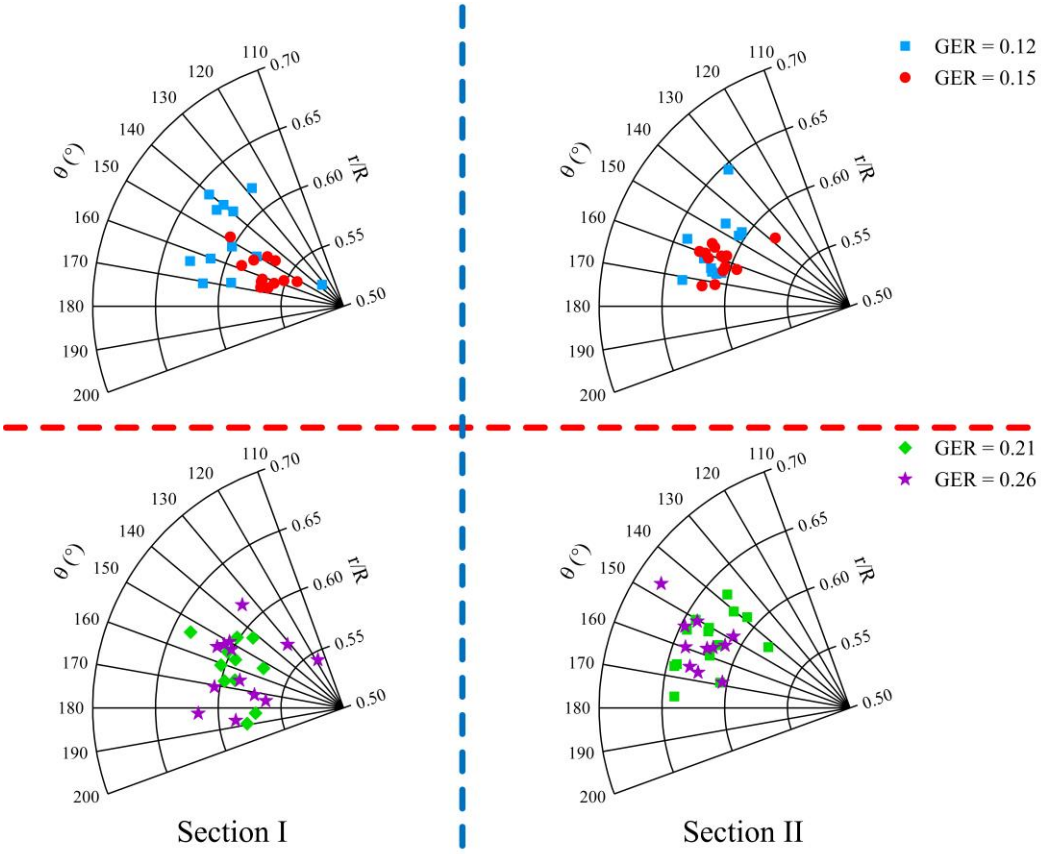

Fig. 6 Distribution of instantaneous OH-PLIF signal intensity centers in the polar coordinate system.

Fig. 7 presents the time-averaged OH-PLIF and flame distribution probability images with different GER. In order to clarify their physical meaning, the method to generate such images with GER = 0.12 at the middle section of the combustor is introduced as an example. The time-averaged OH-PLIF images are generated by averaging all the instantaneous OH-PLIF images. The method to produce the flame distribution probability images is: (1) Binarize all the instantaneous OH-PLIF images. The pixel points where the flame exists are assigned a value of 1. (2) Sum all the binarized images and then divide by the total number of binarized images. Therefore, the value at each pixel represents the local existing probability of the flame. These images represent the statistical properties of flame structure and combustion intensity. The instantaneous OH-PLIF images shown in Fig. 5 present an irregular flame loop that is constantly evolving over time due to turbulent disturbance. Nevertheless, Fig. 7 exhibits a roughly regular flame loop with relatively smooth edges with different GER at any section. It suggests that the combustion mainly occurs in a regular loop region in terms of statistical properties. Despite the actual instantaneous flame structure is disturbed by turbulence, it mainly distributes in the loop region. It is a basic property for the combustion in an axisymmetric supersonic combustor.

The flame structure at the middle section of the combustor is discussed first. The loop-shaped region with a flame distribution probability of 0.4 to 1 can be defined as a main flame distribution region, which is essentially coincident with the flame loop presented in the time-averaged OH-PLIF images. It can be regarded as a favorable region for flame stabilization. The flame distribution probability is close to 1 near the center of the loop region, and it decreases rapidly as the loop region spreads out into both the cavity and core flow. Although the fragmented flames occasionally appear outside of the high-probability loop region (as shown in Fig. 5), the local probability is less than 0.2. It means that

the local core flow, as well as cavity recirculation flow, are unfavorable for flame stabilization. Only a small amount of fragmented flames are generated at any instantaneous. The high-probability loop region diffuses with increasing GER, which compresses the core flow marked by the central hollow region. The instantaneous OH-PLIF images shown in Fig. 5 present a fragmented loop-shaped flame structure when GER exceeds 0.21. Despite the statistical operation somewhat eliminating the instantaneous details, the flame distribution probability also shows a fragmented loop morphology. It indicates that the flame structure at the middle part of the combustor is unsteady due to thermal choking. In addition, the high-probability loop region is expanded with this condition. Some fragments near the periphery of the loop region spread to the core flow and cavity. It means that the amount of fragmented flames increases dramatically and spreads outside the loop region.

As noted above, the flow conditions for combustion near the ramp are much more favorable than the middle part of the combustor. It can be seen that the flame distribution is expanded, and the combustion intensity is enhanced significantly from the time-averaged OH-PLIF images. The loop region with a flame distribution probability close to 1 is expanded dramatically, which compresses the core flow by nearly 20%~30%, compared to the middle section with the same GER. The core flow is almost filled with a great number of fragmented flames. It increases the local flame distribution probability to more than 0.4. Moreover, when the combustion instability occurs induced by thermal choking as GER exceeds 0.21, the flame structure integrity near the ramp is affected slightly, as shown in flame distribution probability. It is significantly different from the fragmented flame structure at the middle section. Thus, the combustion is more steady near the ramp.

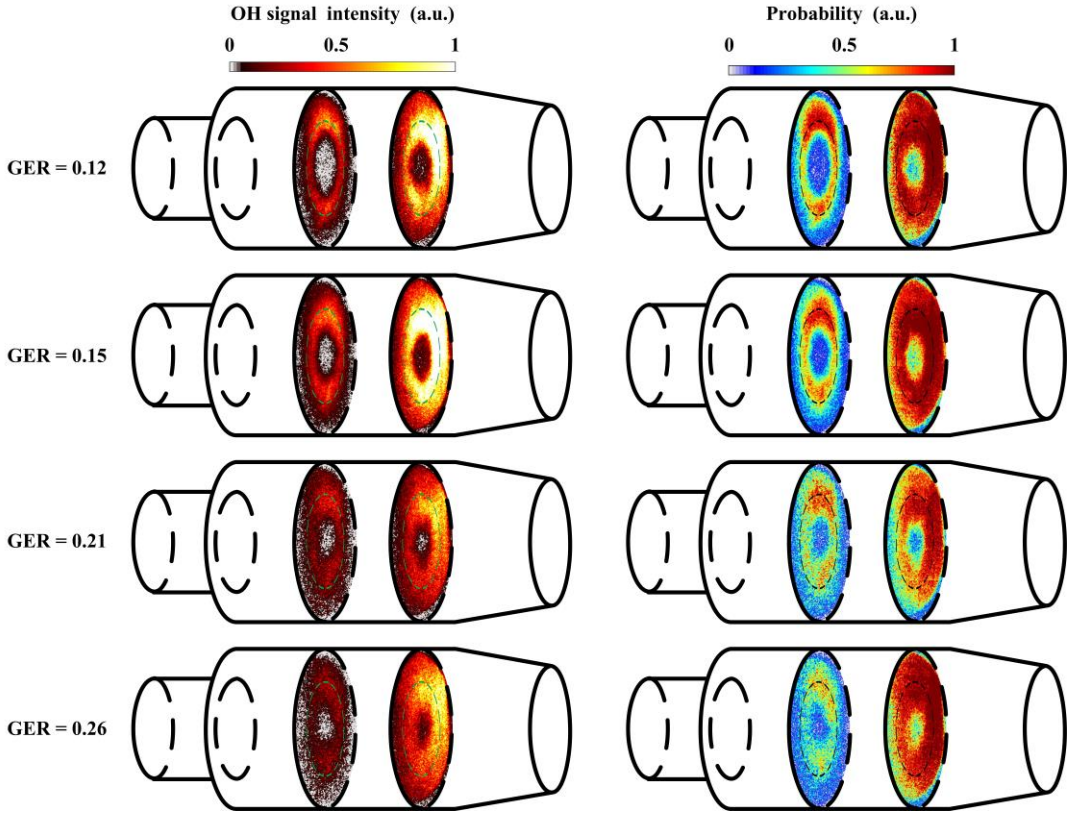

Fig. 7 Time-averaged OH-PLIF images and flame distribution probability images with different GER.

Fig. 8 presents the radial distribution curves of the OH-PLIF time-averaged signal intensity. There are two types of curve shapes shown in Fig. 8. One exhibits a much higher intensity inside the flame loop than the core flow when GER is less than 0.15. It means that the combustion without thermal choking occurs mainly near the loop-shaped cavity shear-layer. Another type shows a relatively smooth curve when GER exceeds 0.21. The flame loop is expanded and the combustion is diminished, compared to GER = 0.15. It is a result of thermal choking that promotes flame to propagate upstream the cavity. However, the combustion is enhanced in the core flow simultaneously since a great amount of fragmented flames appear there. Therefore, the OH signal intensity is roughly equivalent in the core

flow and flame loop. This type of curve shape can be regarded as a characterization of thermal choking. The conditions for combustion near the ramp are more conducive than the middle part of the combustor. The OH signal intensity in the flame loop near the ramp is 1.5~2 times stronger than the middle part with the same GER. In addition, the intensity in the core flow is 3~5 times stronger. The remarkably enhanced combustion near the core flow suggests a severe thermal choking near the ramp.

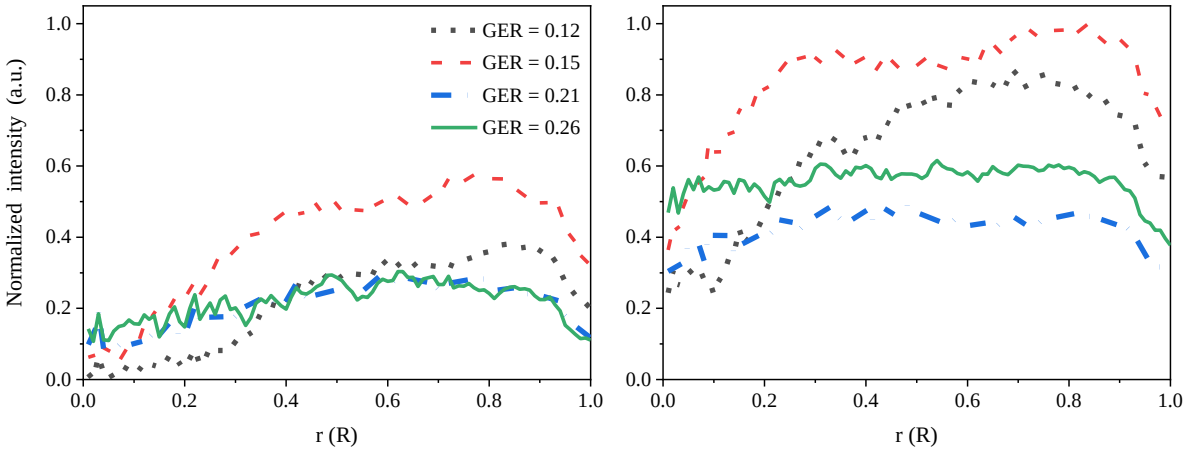

Fig. 8 Radial distribution curves of the OH-PLIF time-averaged signal intensity.

4. Conclusions

The characterizations and evolving laws of the flame structure during combustion destabilization in an axisymmetric supersonic combustor were investigated with multi-view OH-PLIF imaging. The experiments were conducted in a fully transparent axisymmetric supersonic glass combustor with an inflow speed of Mach 2.5 and a total temperature of 1800 K. The circumferential and axial flame structures with different GER were visualized and analyzed. The high-speed photography and pressure measurement systems were employed to assist in the analysis of the flame structure evolution during combustion destabilization. The main conclusions are as follows:

(1) A loop-shaped flame with a central hole is generated by the axisymmetric supersonic combustor. There is an approximately regular loop region near the cavity shear-layer where the combustion mainly occurs from a time-averaged perspective. The instantaneous flame structure fluctuates over time in this loop region. It shows an irregular loop-shaped morphology with a wrinkled and distorted profile caused by strong turbulent disturbances. The flame loop is thickened along the cavity shear-layer, which compresses the core flow significantly downstream and impinges on the ramp to spread into the cavity. The combustion is most intense near the ramp. The local core flow is decelerated sharply, enabling a considerable amount of fragmented flames to burn in the apparently compressed central hole.

(2) The combustion stabilization is enhanced with an appropriate increase in GER. The excessive enhanced combustion triggers thermal choking as GER exceeds 0.21. The flame propagates upstream away from the cavity along the boundary-layer near the hydrogen jet wake. It leads to a violent reciprocal flame propagation, marking an unsteady combustion. The thermal choking initiates near the ramp where the most intense combustion occurs. The local flame loop is significantly expanded, filling almost the entire flow path. The loop-shaped flame structure downstream the combustor is affected slightly due to a favorable local environment for combustion with a low-speed and thickened cavity shear-layer. In contrast, the reciprocal flame propagation upstream the cavity disrupts the flame structure near the middle part of the combustor. A diffused and fragmented flame loop fluctuates violently over time. A large amount of fragmented flames spread into the core flow occasionally.

Acknowledgments

This work is supported by the National Natural Science Foundation of China (NSFC) (Nos. 11925207, 12322211, 12172379, 92252206) and the Youth Independent Innovation Science Found Project of the National University of Defense Technology (No. ZK23-40).

References

1. Castrogiovanni, A.: The scramjet engine, processes and characteristics. AIAA J. (9), 2173-2174 (2010)
2. Qin, F., Z. Huang, G. He, S. Wang, X. Wei and B. Liu.: Flame stabilization mechanism study in a hydrogen-fueled model supersonic combustor under different air inflow conditions. Int. J. Hydrog. Energy. 42(33), 21360-21370 (2017)
3. Du, G., Y. Tian, J. Le, F. Zhong and Y. Zhang.: Experimental investigation of effects of dual-cavity configuration on ignition and flame stabilization in a kerosene-fueled supersonic combustor. Phys. Fluids. 35(1), 15138 (2023)
4. Miao, H., Z. Zhang, Y. He, Y. Wu, M. Jia, W. Cui and Y. Li.: Ignition enhancement of liquid kerosene by a novel high-energy spark igniter in scramjet combustor at Mach 4 flight condition. Aerosp. Sci. Technol. 139(0), 108397 (2023)
5. Wu, C., F. Zhong and J. Fan.: An analytical theory of heated duct flows in supersonic combustors. Theor. Appl. Mech. Lett. 4(3), 032001 (2014)
6. Tian, Y., S. Tong, D. Wu, H. Ren, C. Hao, M. Guo, X. Deng, J. Le and H. Zhang.: Reconstructing the flame in supersonic combustion flow by using the distribution of the wall pressure based on deep learning. Phys. Fluids. 35(6), (2023)
7. Chang, J., J. Zhang, W. Bao and D. Yu.: Research progress on strut-equipped supersonic combustors for scramjet application. Prog. Aeosp. Sci. 103(1), 1-30 (2018)
8. Zhang, J., J. Chang, W. Shi, W. Hou and W. Bao.: Combustion stabilizations in a liquid kerosene fueled supersonic combustor equipped with an integrated pilot strut. Aerosp. Sci. Technol. 77, 83-91 (2018)
9. Liu, Q., D. Baccarella and T. Lee.: Review of combustion stabilization for hypersonic airbreathing propulsion. Prog. Aeosp. Sci. 119(No.0), 100636 (2020)
10. Zheng, S., W. Cai, B. Liu, S. Zhu, B. Zhou, R. Sui and Q. Lu.: Experimental detection of two-dimensional temperature distribution in Rocket-Based Combined Cycle combustion chamber using multispectral imaging processing. Fuel. 333, 126391 (2023)
11. Aguilera, C. and K. H. Yu.: Scramjet to ramjet transition in a dual-mode combustor with fin-guided injection. Proc. Combust. Inst. 36(2), 2911-2918 (2017)
12. Fiévet, R., S. Voelkel, H. Koo, V. Raman and P. L. Varghese.: Effect of thermal nonequilibrium on ignition in scramjet combustors. Proc. Combust. Inst. 36(2), 2901-2910 (2017)
13. Fang, J., X. Deng and Z. X. Chen.: Direct numerical simulation of supersonic internal flow in a model scramjet combustor under a non-reactive condition. Phys. Fluids. 35(2), (2023)
14. Zhang, D. and W. Song.: Experimental study of cone-struts and cavity flameholders in a kerosene-fueled round scramjet combustor. Acta Astronaut. 139, 24-33 (2017)
15. Chang, J., J. Zhang, W. Bao and D. Yu.: Research progress on strut-equipped supersonic combustors for scramjet application. Prog. Aeosp. Sci. 103, 1-30 (2018)
16. Zhang, J., J. Chang, F. Quan, L. Bian and W. Bao.: Ignition characteristics in a thin strut-equipped dual mode combustor fueled with liquid kerosene. Acta Astronaut. 161, 125-138 (2019)
17. Nakaya, S., Y. Hikichi, Y. Nakazawa, K. Sakaki, M. Choi, M. Tsue, M. Kono and S. Tomioka.: Ignition and supersonic combustion behavior of liquid ethanol in a scramjet model combustor with cavity flame holder. Proc. Combust. Inst. 35(2), 2091-2099 (2015)
18. Li, F., T. Wang, K. Yang, J. Zhang, H. Wang, M. Sun, Z. Wang and P. Li.: Effect of fuel temperature on mixing characteristics of a kerosene jet injected into a cavity-based supersonic combustor. Phys. Fluids. 35(4), (2023)
19. Kim, K. M., S. W. Baek and C. Y. Han.: Numerical study on supersonic combustion with cavity-based fuel injection. Int. J. Heat Mass Transf. 47(2), 271-286 (2004)
20. Sun, M., Z. Wang, J. Liang and H. Geng.: Flame Characteristics in Supersonic Combustor with Hydrogen Injection Upstream of Cavity Flameholder. J. Propul. Power. 24(4), 688-696 (2008)
21. Wang, H., Z. Wang, M. Sun and H. Wu.: Combustion modes of hydrogen jet combustion in a cavity-based supersonic combustor. Int. J. Hydrog. Energy. 38(27), 12078-12089 (2013)

22. Li, F., M. Sun, Z. Cai, Y. Sun, F. Li, J. Zhang and J. Zhu.: Experimental study of flame stabilization in a single-side expansion scramjet combustor with different cavity length-to-depth ratios. Acta Astronaut. 173, 1-8 (2020)
23. Sun, M., H. Geng, J. Liang and Z. Wang.: Mixing Characteristics in a Supersonic Combustor with Gaseous Fuel Injection Upstream of a Cavity Flameholder. Flow, turbulence and combustion. 82(2), 271-286 (2009)
24. Li, X., W. Liu, Y. Pan, L. Yang, B. An and J. Zhu.: Characterization of kerosene distribution around the ignition cavity in a scramjet combustor. Acta Astronaut. 134, 11-16 (2017)
25. McGann, B., C. D. Carter, T. M. Ombrello, S. Hammack, T. Lee and H. Do.: Gas property measurements in a supersonic combustor using nanosecond gated laser-induced breakdown spectroscopy with direct spectrum matching. Proc. Combust. Inst. 36(2), 2857-2864 (2017)
26. Zhao, G., M. Sun, J. Wu, X. Cui and H. Wang.: Investigation of flame flashback phenomenon in a supersonic crossflow with ethylene injection upstream of cavity flameholder. Aerosp. Sci. Technol. 87, 190-206 (2019)
27. Ma, G., M. Sun, G. Zhao, C. Liang, H. Wang and J. Yu.: Effect of injection scheme on asymmetric phenomenon in rectangular and circular scramjets. Chin. J. Aeronaut. 36(1), 216-230 (2023)
28. Tang, T., G. Zhao, H. Wang, M. Sun and Z. Wang.: Effects of cavity parameters on flame flashback phenomenon in a supersonic crossflow with a cavity flameholder. Proceedings of the Institution of Mechanical Engineers, Part G: Journal of Aerospace Engineering. 237(7), 1582-1599 (2023)
29. Liu, Q., D. Baccarella, B. McGann and T. Lee.: Cavity-enhanced combustion stability in an axisymmetric scramjet model. AIAA J. 57(9), 3898-3909 (2019)
30. Liu, Q., D. Baccarella, W. Landsberg, A. Veeraragavan and T. Lee.: Cavity flameholding in an optical axisymmetric scramjet in Mach 4.5 flows. Proc. Combust. Inst. 37(3), 3733-3740 (2019)
31. Qiu, H., J. Zhang, G. Feng, J. Chang and W. Bao.: Numerical Investigation on Performance of Axisymmetric Variable Geometry Scramjet Combustor Equipped with Strut Flame Holder. Combust. Sci. Technol., 1-25 (2021)
32. Liu, Q., D. Baccarella, B. McGann and T. Lee.: Dual-mode operation and transition in axisymmetric scramjets. AIAA J. 57(11), 4764-4777 (2019)
33. Micka, D. J. and J. F. Driscoll.: Combustion characteristics of a dual-mode scramjet combustor with cavity flameholder. Proc. Combust. Inst. 32(2), 2397-2404 (2009)
34. Aguilera, C. and K. H. Yu.: Scramjet to ramjet transition in a dual-mode combustor with fin-guided injection. Proc. Combust. Inst. 36(2), 2911-2918 (2017)
35. Landsberg, W. O., T. Vanyai, T. J. McIntyre and A. Veeraragavan.: Experimental scramjet combustion modes of hydrocarbon mixtures at Mach 8 flight conditions. AIAA J. 58(12), 5117-5122 (2020)
36. Landsberg, W. O., T. Vanyai, T. J. McIntyre and A. Veeraragavan.: Dual/scram-mode combustion limits of ethylene and surrogate endothermically-cracked hydrocarbon fuels at Mach 8 equivalent high-enthalpy conditions. Proc. Combust. Inst. 38(3), 3835-3843 (2021)
37. Vanyai, T., W. O. Landsberg, T. J. McIntyre and A. Veeraragavan.: OH visualization of ethylene combustion modes in the exhaust of a fundamental, supersonic combustor. Combust. Flame. 226, 143-155 (2021)
38. Baccarella, D., Q. Liu, B. McGann, G. Lee and T. Lee.: Isolator-combustor interactions in a circular model scramjet with thermal and non-thermal choking-induced unstart. J. Fluid Mech. 917, (2021)
39. Li, Q., J. Zhu, Y. Tian, M. Sun, M. Wan, B. Yan, T. Luo, Y. Sun, C. Wang, T. Tang and H. Wang.: Investigation of ignition and flame propagation in an axisymmetric supersonic combustor with laser-induced plasma. Phys. Fluids. 35(12), 125133 (2023)